Research Article

Ocular manifestations of central insulin resistance

Muneeb A. Faiq[1, 2, 3], Trina Sengupta[4], Madhu Nath[5], Thirumurthy Velpandian[5], Daman Saluja[3], Rima Dada[6], Tanuj Dada[1, *], Kevin C. Chan[2, *]

From the Contents

Graphical Abstract

Blocking insulin receptor in the central nervous system by S961 injection may lead to neurodegenerative phenotype in ocular structures without remarkable alterations in blood glucose or serum insulin
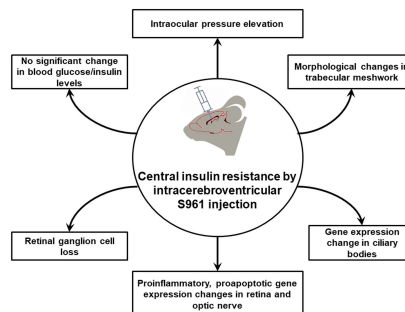
Abstract

Central insulin resistance, the diminished cellular sensitivity to insulin in the brain, has been implicated in diabetes mellitus, Alzheimer's disease and other neurological disorders. However, whether and how central insulin resistance plays a role in the eye remains unclear. Here, we performed intracerebroventricular injection of S961, a potent and specific blocker of insulin receptor in adult Wistar rats to test if central insulin resistance leads to pathological changes in ocular structures. 80 mg of S961 was stereotaxically injected into the lateral ventricle of the experimental group twice at 7 days apart, whereas buffer solution was injected to the sham control group. Blood samples, intraocular pressure, trabecular meshwork morphology, ciliary body markers, retinal and optic nerve integrity, and whole genome expression patterns were then evaluated. While neither blood glucose nor serum insulin level was significantly altered in the experimental or control group, we found that injection of S961 but not buffer solution significantly increased intraocular pressure at 14 and 24 days after first injection, along with reduced porosity and aquaporin 4 expression in the trabecular meshwork, and increased tumor necrosis factor α and aquaporin 4 expression in the ciliary body. In the retina, cell density and insulin receptor expression decreased in the retinal ganglion cell layer upon S961 injection. Fundus photography revealed peripapillary atrophy with vascular dysregulation in the experimental group. These retinal changes were accompanied by upregulation of pro-inflammatory and pro-apoptotic genes, downregulation of anti-inflammatory, anti-apoptotic, and neurotrophic genes, as well as dysregulation of genes involved in insulin signaling. Optic nerve histology indicated microglial activation and changes in the expression of glial fibrillary acidic protein, tumor necrosis factor α, and aquaporin 4. Molecular pathway architecture of the retina revealed the three most significant pathways involved being inflammation/ cell stress, insulin signaling, and extracellular matrix regulation relevant to neurodegeneration. There was also a multimodal crosstalk between insulin signaling derangement and inflammation-related genes. Taken together, our results indicate that blocking insulin receptor signaling in the central nervous system can lead to trabecular meshwork and ciliary body dysfunction, intraocular pressure elevation, as well as inflammation, glial activation, and apoptosis in the retina and optic nerve. Given that central insulin resistance my lead to neurodegenerative phenotype in the visual system, targeting insulin signaling may hold promise for vision disorders involving the retina and optic nerve.

Key Words: brain; ciliary bodies; gene expression; inflammation; insulin receptor; insulin resistance; intraocular pressure; neurodegeneration; optic nerve; retina; retinal ganglion cells; trabecular meshwork

Introduction

Diabetes can play a major role in the progressive damage to the retina (Bao et al., 2020), yet its mechanisms remain under investigation. Although high blood glucose concentration is thought to be the underlying etiology for diabetic retinopathy, hyperglycemia accounts only for around 11% of variability in the risk of disease development (Bronson et al., 2003; Bao et al., 2020) indicating the possible involvement of other factors for the disease. Insulin resistance is a condition in which the cells of the body become less sensitive to the effects of insulin due to loss and/or insensitivity of insulin receptors (InRs). It is seen in both type 1 and type 2 diabetes (Bao et al., 2020), whereby IR cells of the body have built up a tolerance to insulin, making the hormone less effective. While peripheral insulin resistance can lead to hyperglycemia, insulin resistance without hyperglycemia has been reported along with retinal lesions that are characteristic of diabetic retinopathy (Bronson et al., 2003; Rajagopal et al., 2016; Bao et al., 2020), indicating that insulin sensitizers may offer therapeutic options to certain conditions in the eye without hyperglycemia. However, recent attempts to examine the effects of insulin signaling on the retina involve systemic administration of insulin, insulin agonists, or insulin sensitizers, which can lower blood glucose levels and cannot tease out the effects of blood glucose from those of insulin signaling networks in contributing to diabetes and other ocular diseases. There is an unmet need of a more specific model of insulin resistance on the retina independent of hyperglycemia in order to understand how such conditions can affect the eye.

Since the eyes are an extension of the brain with similarities in terms of embryology, histology, tissue organization, and cerebrospinal fluid circulation (Barishak, 1992; Cvekl and Tamm, 2004; Lamb et al., 2007; Langenberg et

[1]Dr. Rajendra Prasad Centre for Ophthalmic Sciences, All India Institute of Medical Sciences, New Delhi, India; [2]Neuroimaging and Visual Science Laboratory, Department of Ophthalmology, NYU Grossman School of Medicine, NYU Langone Health, New York University, New York, NY, USA; [3]Medical Biotechnology Laboratory, Dr. B. R. Ambedkar Center for Biomedical Research, University of Delhi, Delhi, India; [4]Dr. Baldev Singh Sleep Laboratory, Department of Physiology, All India Institute of Medical Sciences, New Delhi, India; [5]Department of Ocular Pharmacology, Dr. Rajendra Prasad Center for Ophthalmic Sciences, All India Institute of Medical Sciences, New Delhi, India; [6]Laboratory for Molecular Reproduction and Genetics, Department of Anatomy, All India Institute of Medical Sciences, New Delhi, India
*Correspondence to: Tanuj Dada, MD, tanujdada@gmail.com; Kevin C. Chan, PhD, chuenwing.chan@fulbrightmail.org.
https://orcid.org/0000-0002-3111-396X (Tanuj Dada); https://orcid.org/0000-0003-4012-7084 (Kevin C. Chan)

al., 2008; Faiq et al., 2014, 2016), it is plausible that insulin resistance in the central nervous system can involve pathological expressions in the optic nerve, retina, and other ocular structures (Galvis et al., 2016; Liu et al., 2017; Zarei et al., 2017; Bao et al., 2020). Apart from diabetes, metabolic and cognitive disorders such as Alzheimer's disease may also involve central insulin resistance (Talbot, 2014; Arnold et al., 2018). Recent studies have used intracerebral streptozotocin injection to establish insulin failure in the brain (Grieb, 2016; Moreira-Silva et al., 2019). However, these studies have pertinent drawbacks including non-specificity of free radical damage by streptozotocin. To test the hypothesis that blocking insulin signaling in the central nervous system leads to neurodegenerative phenotype in ocular structures without remarkable alterations in blood glucose or serum insulin, it is, therefore, important to inhibit specifically the InRs in the central nervous system. To achieve this goal, this study used a specific InR blocker S961 to establish central insulin resistance in an experimental rat model. We evaluated its effects on the intraocular pressure, the integrity of anterior and posterior segments in the eye, and gene and protein expression in the retina and optic nerve.

Methods

Animals
Twenty-four healthy male Charles River Wistar rats with no previous experimental or drug exposure (5–6 months old, 200–250 g, procured, bred and single-housed at the animal facility of All India Institute of Medical Sciences, New Delhi, India) were randomly divided into two groups: experimental S961 (n = 12) and sham control (n = 12) using the sealed envelope method. All animals were housed under standard conditions of a 12-hour light-dark cycle, 24 ± 1°C temperature and 62 ± 5% humidity. The rats were provided with standard chow and water *ad libitum*. All animals received surgery for cannula implantation into the lateral ventricle. One week later, six animals from the experimental group were randomly selected to receive intracerebroventricular injection of the S961 solution while another six animals from the sham control group received intracerebroventricular injection of the buffer solution. After *in vivo* assessments for about 3 weeks, these animals were then sacrificed for histology at 24 days after intracerebroventricular injection. The other six animals in each group were sacrificed for tissue collections at baseline after cannula implantation but without S961 or buffer solution injection. The study was approved by the Institutional Animal Ethics Committee at All India Institute of Medical Sciences, New Delhi, India (approval No. 794/IAEC/14, approval date: August 12, 2014) and the Institutional Animal Care and Use Committee at New York University Grossman School of Medicine (approval No. IA17-00370). All experiments were performed in accordance with the guidelines of the Association for Research in Vision and Ophthalmology (ARVO) for the Use of Animals in Ophthalmic and Vision Research. An overview of the experimental paradigm is depicted in **Figure 1A**.

Surgery
Under anesthesia by intraperitoneal injection of sodium pentobarbital (25 mg/mL concentration, 40 mg/kg body weight), a 24 gauge, 15 mm long guide cannula with an indwelling stylet was stereotaxically implanted in either the left or right lateral ventricle chosen randomly through a burr hole in the skull at 0.5 mm posterior to the coronal suture, 2 mm lateral to the sagittal suture and 3 mm below the dura mater with reference to the De Groot atlas (Seyer et al., 2016; **Figure 1B** and **C**). The cannula was held in place by dental cement. All the surgical procedures were carried out following the 3R (replacement, reduction, and refinement) rule of aseptic technique (Ferry and Gervasoni, 2021). After a 7-day post-surgical recovery period, 1 mg/μL of S961 (CAS# 1083433, Sigma-Aldrich, St. Louis, MO, USA) solution or buffer solution (1× phosphate buffered saline) was injected at the rate of 1 μL/min over 80 minutes into the lateral ventricle of a subset of animals (experimental group: n = 6; control group: n = 6) twice at 7 days apart. Post-surgical care was performed by monitoring the animals for any complications, change in behavior or infections. No antibiotic prophylaxis was used in post-surgical care.

Blood glucose and serum insulin levels
Blood samples were collected by venipuncture at the tail base using 21–23 gauge needles at baseline and/or at 24 days for all living animals before sacrifice, and the serum was isolated and stored at −80°C until further use. Blood glucose levels were estimated using ACCU-CHEK Compact Plus (Roche Diagnostics, Kagaku Kenkyusho, Japan; sensitivity 81%, Kermani et al., 2017) calibrated for plasma glucose levels and the results were expressed as mg/dL. Serum insulin levels were quantified using AccuLite CLIA Microwells kit (Cat# 2425-300, Monobind Inc. Lake Forest, CA, USA; sensitivity 0.182 μIU/mL) and the results were expressed as mU/L (Patel et al., 2016).

Tonometry
Intraocular pressure was assessed with TonoPen XL (Reichert Technologies, Inc, Depew, NY, USA) over 24 days at the same time of the day to avoid any diurnal variations. The intraocular pressure was recorded within the first 3 minutes after induction of anesthesia by inhaled isoflurane (Henry Schein Inc., Melville, NY, USA; 3% induction and 1–1.5% maintenance with a flow rate of 0.4–0.8 L/min) under 0.5% proparacaine topical eye drops. The average of five readings were taken for each eye at each time point, and the average value of both eyes was then obtained for each animal for comparisons over time and between groups.
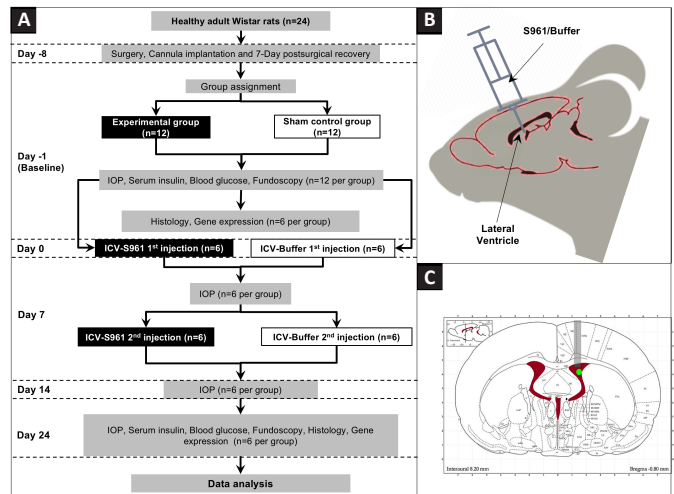
Figure 1 | Overall experimental paradigm.
(A) Experimental procedure flow chart before and after intracerebroventricular (ICV) S961 or buffer solution injection on day 0. (B) Schematic diagram of the site of S961 or buffer injection in the lateral ventricle of the rat brain in the sagittal view. (C) Rat brain atlas (http://labs.gaidi.ca/rat-brain-atlas/) at the level of the lateral ventricles (red) in the coronal view. The grey bar represents the location of cannula implantation for S961 or buffer delivery. The green dot indicates the site of injection in the right lateral ventricle. IOP: Intraocular pressure.

Color fundus photography
Fundoscopy of the rat eyes was acquired *in vivo* after taking IOP measurements using the Micron III retinal imaging system (Phoenix Research Labs, Pleasanton, CA, USA) under anesthesia with 1–1.5% isoflurane with body temperature maintained at 37°C on a heating pad. The pupils were dilated with topical administration of tropicamide (IndiaMart, Delhi, India; 5 mg/mL), and the camera was adjusted to focus on the optic nerve head. We waited 8 hours after tropicamide exprosure and fundoscopy before sacrificing the animals for tissue harvest at baseline or 24 days.

Tissue collection
After sacrificing the animals, the eyes and optic nerves were harvested. The tissues from one eye and both optic nerves were first fixed with solutions containing 2% formaldehyde and 2.5% glutaraldehyde at a 3:1 ratio. They then underwent paraffin embedding and cryotome/microtome sectioning in various planes (VT 1000 S, Leica, Wetzlar, Germany) at 5 μm thickness for histology (including H&E staining, retinal ganglion cell labeling and immunofluorescence) and at 1 μm thickness for electron microscopy. The prepared tissue sections were stored at 4°C until further analyses. The tissues from the other eye were used for gene expression studies (including microarray and polymerase chain reaction analyses of the retina).

Hematoxylin and eosin staining of the retina
The prepared 5 μm-thick tissue sections were brought to room temperature and deparaffinized. The tissue sections were then stained with hematoxylin (Bio Lab Diagnostics, Mumbai, India) for 15 minutes and counterstained with 1% eosin (Bio Lab Diagnostics) for another 15 minutes. After dehydration by treating with ethanol at 50% concentrations for 2 minutes, 65% for 2 minutes, 85% for 2 minutes, 90% for 2 minutes, 100% for 10 minutes, xylene: ethanol (1:1) for 6 minutes and xylene for 6 minutes, sections were observed at 400× magnification under a light microscope (Olympus BX51TF microscope with DP70 color camera, Olympus, Tokyo, Japan). The cell density of the retina was evaluated by counting the number of neuronal cells per 0.1 mm^2 area using the Cell Counter plugin of ImageJ v1.47 (Rasband, W.S., National Institutes of Health, Bethesda, MD, USA).

Retinal ganglion cell labeling
Retrograde labeling of the retinal ganglion cells was done by direct stereotaxic injection of biotinylated rhodamine-dextran (Cat# D7135, ThermoFisher Scientific, Waltham, MA, USA) (4 μL) by unilateral direct stereotaxic injection into the optic nerve (Nadal-Nicolas et al., 2015) followed by a 3-day wait. Visualization was done with epifluorescent illumination using a fluorescence microscope (Nikon eclipse Ti fluorescence microscope, Nikon, Tokyo, Japan). With the plane of focus in the ganglion cell layer, a 400 μm × 400 μm field of retinal ganglion cells were captured. The cells were illuminated using a 20× objective and with the partially closed epilluminator aperture.

Immunofluorescence of the trabecular meshwork, ciliary body, retina, and optic nerve
Slides prepared from tissue sections were brought to room temperature, deparaffinized, and rehydrated by treating with xylene for 6 minutes, xylene:ethanol (1:1) for another 6 minutes, ethanol at 100% concentrations for 2 minutes, 85% for 2 minutes, 65% for 2 minutes, 50% for 2 minutes and phosphate-buffered saline (PBS) twice for 5 minutes. The sections were then permeabilized with 0.1% Triton X-100 solution (Cat# 388858, Sigma) at 25°C for 10 minutes, washed with PBS twice for 5 minutes, blocked with 3–5% BSA (prepared with PBST; phosphate-buffered saline tween) for 45

minutes at 37°C, and then incubated for 12 hours at 4°C with the primary antibody for InR (SC-711, rabbit polyclonal, Santa Cruz Biotechnology, Inc. RRID:AB_631835), aquaporin 4 (AQP4; a marker for water channel) (SC-20812, rabbit polyclonal, Santa Cruz Biotechnology, Inc, RRID: AB-2274338), tumor necrosis factor α (TNFα; a marker for inflammation) (SC-8301, rabbit polyclonal, Santa Cruz Biotechnology, Inc. RRID: AB_2303410), and optic atrophy protein 1 (OPA1; a marker for optic neuropathy) (NB110-55290, rabbit polyclonal, Novus Biologicals, RRID: AB-829789). After washing with PBS and PBST, sections were incubated for 1 hour at room temperature with the corresponding HRP-conjugated goat anti-rabbit IgG secondary antibody (SC-2004; Santa Cruz Biotechnology, Inc. RRID: AB-631746). The sections were then observed under a fluorescence microscope (Nikon eclipse Ti fluorescence microscope, Nikon). The relative expression was measured based on the fluorescence intensity using ImageJ v1.47 (National Institutes of Health, Bethesda, MD, USA; Schneider et al., 2012).

Electron microscopy of the trabecular meshwork and optic nerve
After harvesting the eyes, tissues were excised near the limbus at the trabecular meshwork and at the optic nerve head. They were then mounted on metal stubs, sputter-coated with 20 nm thick colloidal gold (CAS# 7440-57-5, Sigma), and examined under a scanning electron microscope (Leo 435 VP system, Oberkochen, Germany) and a transmission electron microscope (Philips, Model CM 10, Eindhoven, the Netherlands). Using the secondary electron mode, direct three-dimensional images were captured at the magnification of 200×, 500×, 3000×, and 4000×. The pore size of the trabecular meshwork was estimated by thresholding and binarization using the ImageJ v1.47 software. Only the diameter of the pore but not the pore volume was assessed due to the lack of depth measurements along the z-axis.

Microarray analysis of the retina
RNA was isolated by homogenizing individual retinas in 1 mL Trizol (Ambion, Austin, Texas, USA) and 200 µL chloroform (Merck, Steinheim, Germany) followed by the collection of 500 µL aqueous phase and treatment with 500 µL of isopropanol (CAS# 67-63-0, Merck) (Wohlfart et al., 2014). RNA pellets were obtained by centrifugation at 16,000 × g, washed with 80% ethanol three times, and stored in 30 µL of diethyl pyrocarbonate (CAS# 1609-47-8, Merck). Whole genome expression profiling was performed using arrays of RaGene-1_0-st-v1-type from Affymetrix (Santa Clara, CA, USA) (Okoniewski et al., 2007; Lee et al., 2009; Pohl et al., 2009). Biotinylated antisense cRNA was then prepared by *in vitro* transcription reaction with BioArrayTMHighYieldTMRNA Transcript Labeling Kit (ENZO Life Science, Lausen, Switzerland, Cat# ENZ-42655; Boothroyd et al., 2007) followed by hybridization, dyeing with a fluidics station, scanning, and analysis using the Agilent Genespring 13.1.1 software (http://www.agilent.com/en/product/software-informatics/genomics-software-informatics/gene-exoression/genespring-gx). MetaCore analysis (https://portal.genego.com/) was employed to identify differentially expressed genes using unpaired t-tests and Benjamin Hochberg correction with a false discovery rate of $P < 0.01$. Network analysis was performed on selected genes with a fold change of >1.5 using the same MetaCore analysis software.

Real-time polymerase chain reaction analysis of the retina
To further validate the results obtained from microarray analysis, quantitative analysis of gene expression after S961 or buffer injection was performed by the CFX96 Real Time System (Bio-Rad, Hercules, CA, USA) using SsoFastTMEvaGreenSupermix (Bio-Rad, Cat# 172-5200). Primers were designed using the Gene runner software 64-Bit version 6.5.52 (http://www.generunner.net/). Similar to the network analysis, the selected genes were determined based on a fold change cut-off of > 1.5 differentially expressed genes with unpaired t-tests and Benjamin Hochberg corrections with a false discovery rate of $P < 0.05$. Amplification reactions were performed in a 20 µL final volume containing 10 µL SsoFastTMEvaGreensupermix, 1 µL primer, and 4 µL cDNA. The quantitative reverse transcription-polymerase chain reaction conditions were as follows: incubation at 55°C for 20 minutes, followed by PCR cycling which included initial denaturation at 95°C for 3 minutes, followed by 35 cycles at 95°C for 15 seconds and 60°C for 48 seconds. Selected genes were amplified using the primer sets listed in **Table 1**. To normalize the amount of expressed mRNA, the internal housekeeping gene 36B4 was used and each cDNA product was tested in triplicate. The relative quantification of target genes was normalized to β-actin and expressed as ΔCt and fold change (2-ΔΔCt) using volcano plots in the gene expression and network analyses (Livak and Schmittgen, 2001).

Statistical analysis
Unless otherwise specified, statistical analyses were performed using two-way analysis of variance followed by Tukey's honest significant difference *post hoc* test via STATA14 (JMP Statistical Discovery, Houston, TX, USA). Data are presented as the mean ± SEM. Results were considered statistically significant when $P < 0.05$.

Results

Blood glucose and serum insulin levels
As shown in **Figure 2**, no hyperglycemia was observed in either experimental or control group at any time point (all $P > 0.05$). No significant difference in the serum insulin level was observed between experimental and control groups, or between 24 days post-injection and baseline (all $P > 0.05$). No significant baseline difference in blood glucose or serum insulin level was either observed in animals sacrificed at baseline *versus* 24 days (all $P > 0.05$, data not shown).

Table 1 | Sequence of the primers used for real time polymerase chain reaction (PCR) of genes selected for validation after microarray expression analysis

| No.	Gene	Primer (5'–3')	Product length (bp)	Accession number
1	IL2	F: TCT GCA GCG TGT GTT GGA TT	143	NM_053836.1
		R: CTG GCT CAT CAT CGA ATT GGC		
2	IL4	F: GTA CCG GGA ACG GTA TCC AC	282	NM_201270.1
		R: GTG AGT TCA GAC CGC TGA CA		
3	GSK3a	F: CTA CTC CAG TGG GGA GAA GAA	481	NM_017344.2
		R: TGG CGT CCC TAG TAC CTT GA		
4	MAPK15	F: GCC GAA GGA TGT TTG GCA TC	261	XM_006241779.4
		R: GGG GAG AGA GGC TCA GAG AA		
5	FGFR1	F: GTA TCC ATG GAG GTG CGG AG	504	XM_017600255.2
		R: ACA GGC CTA CGG TTT GGT TT		
6	GSK3b	F: AGC TGA TCT TTG GAG CCA CC	596	NM_032080.1
		R: TGG GGC TGT TCA GGT AGA GT		
7	IGF2	F: CAC CTC GCT GCT AAC TCC C	396	NM_031511.2
		R: CTT CGA AGG ATC GAG GAC GG		
8	BCL2L11	F: CTG CTT TCA CTT CGC TCC CC	550	NM_171988.3
		R: GGG CTC CTG TCT GTG TCA AA		
9	NF-kb1A	F: GAG ACC TGG AGC AAG CCA TT	416	NM_199267.2
		R: CAG GCT AGG GTC AGC GTA TG		
10	PI3K	F: AGT GGC CCG GGT AGG TTT	589	NM_001371300.2
		R: TCA GTG ACG TCG TAG CCA AT		
11	NRG1	F: AAG CAG ACA CCA GCT TCA GA	399	NM_001271118.2
		R: ACA GTG CAT TAC CAC GCA GA		
12	IGF1	F: ACC CGG GAC GTA CCA AAA TG	264	NM_178866.4
		R: TCC GGA AGC AAC ACT CAT CC		
13	RARB	F: ATT CGG GGC TGG GAA AAA GA	403	NM_031529.1
		R: ATG ACT TGT CCT GGC AGA CG		
14	InR	F: CGG AGA GGA GAA ACG GGA GA	486	XM_039089096.1
		R: TCT CCA GCT CAT GCA ACCT G		

BCL2L11: B-cell lymphoma-2 like 11; F: forward; *FGFR1*: fibroblast growth factor receptor 1; *GSK3a*: glycogen synthase kinase 3a; *GSK3b*: glycogen synthase kinase 3b; *IGF1*: insulin like growth factor 1; *IGF2*: insulin like growth factor 2; *IL2*; interleukin 2; *IL4*: interleukin 4; *InR*: insulin receptor; *MAPK15*: mitogen-activated protein kinase 15; *NF-kb1A*: nuclear factor kappa B1A; *NRG1*: neuregulin 1; *PI3K*: phosphatidylinositol 3-kinase; R: reverse; *RARB*: retinoic acid receptor beta.
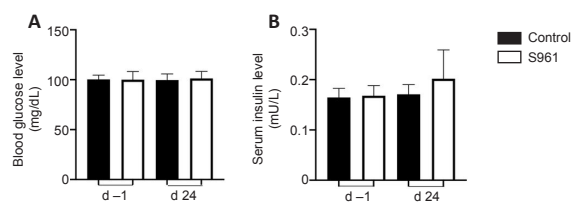
Figure 2 | Blood glucose and serum insulin levels.
(A) Blood glucose levels (mg/dL) at 1 day before (d −1) and 24 days (d 24) after buffer control (black) or experimental S961 injection (white). There was no significant difference in blood glucose levels between experimental and control groups or between time points. (B) Serum insulin levels (mU/L) at −1 and 24 days. There was no statistically significant difference in serum insulin levels between experimental and control groups or between time points, despite a slight increase in the serum insulin level in the S961-injected group at 24 days post-injection. Results are expressed as the mean ± SEM with $n = 6$ per group per time point (two-way analysis of variance followed by Tukey's honest significant difference *post hoc* test; experiments were run in triplicate).

Intraocular pressure and trabecular meshwork morphology
As shown in **Figure 3A**, two-way analysis of variance (ANOVA) of intraocular pressure revealed a statistically significant interaction between the effects of group and time ($F_{(1,19)} = 13.28$, $P = 0.0017$). Tukey's honestly significant difference (HSD) *post hoc* test indicated no significant change in intraocular pressure between groups at baseline or between baseline and 7 days after first intracerebroventricular injection in either group (all $P > 0.05$). However, the experimental S961 group but not the buffer control group showed a significant increase in intraocular pressure at 14 ($P < 0.001$) and 24 days ($P < 0.001$) after the first intracerebroventricular injection, indicating that intraocular pressure elevation did not occur in the experimental group until 2 weeks post-injection and persisted through the end of the experimental period. No significant baseline intraocular pressure difference was observed between animals sacrificed at baseline and animals sacrificed at 24 days (all $P > 0.05$). The trabecular meshwork showed narrowing of the pores and thickening of the beams in the experimental group at 24 days relative to the control group. These changes were accompanied by downregulation of AQP4 with no significant change in GFAP expression as shown in **Figure 3B**.
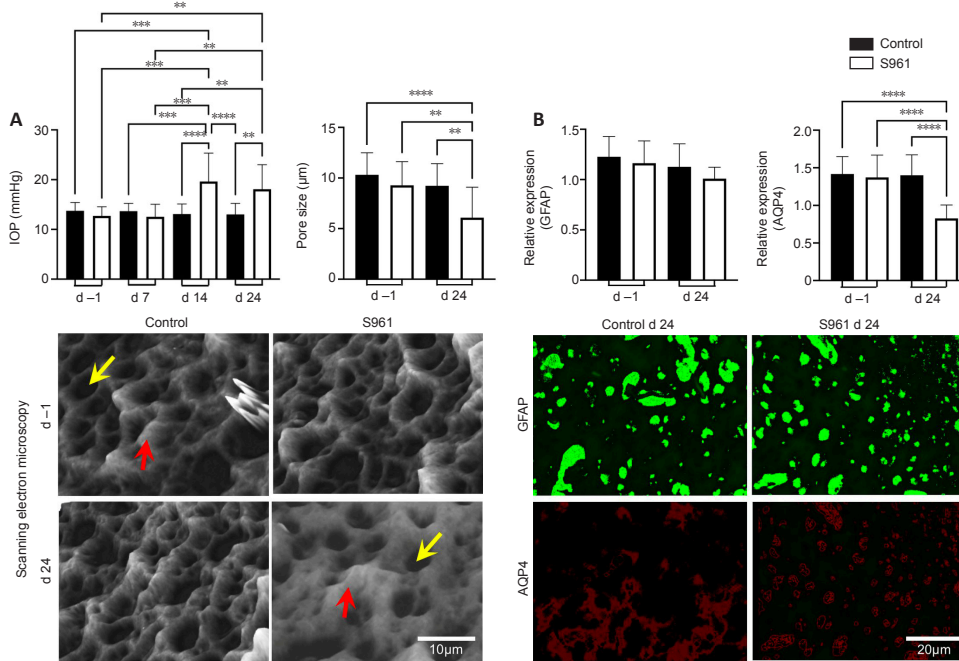
Figure 3 | Changes in intraocular pressure and trabecular meshwork.
(A) (Top left) Intraocular pressure (IOP) of the buffer control (black) and experimental S961 groups (white) at −1 (baseline), 7, 14 and 24 days after intracerebroventricular injection. There was a significant IOP increase at 14 and 24 days relative to −1 and 7 days in the S961-injected group. No significant IOP change was observed in the control group. (Top right) Pore size of the trabecular meshwork at −1 and 24 days in the two groups using scanning electron microscopy (Bottom). At 24 days, the pores (yellow arrows) were apparently decreased in size while the bordering tissues representing the meshwork beams (red arrows) were thickened in the S961-injected animals compared with baseline. No apparent change was observed in the porosity or beam thickness in the trabecular meshwork of the control group between −1 and 24 days. (B) Relative expression of glial fibrillary acidic protein (GFAP) and aquaporin 4 (AQP4) in the trabecular meshwork of both groups at −1 and 24 days. GFAP expression did not show any significant change in either group despite a downward trend for the S961 group. Immunofluorescence images demonstrate similar level of GFAP expression (green) at 24 days in the S961 and control groups. There was, however, a significant decrease in the expression of AQP4 (red) in the trabecular meshwork of the S961 group at 24 days. Results are presented as the mean ± SEM with $n = 6$ per group per time point (two-way analysis of variance followed by Tukey's honest significant difference *post hoc* test: **$P < 0.01$, ***$P < 0.001$, ****$P < 0.0001$; n.s.: not significant; experiments were run in triplicate).

Morphological and immunohistochemical changes in the ciliary body, retina, and optic nerve

Histological examination of the retinal cross sections revealed loss of cells in the ganglion cell layer and dystrophic changes in the photoreceptor layer at 24 days after first intracerebroventricular S961 injection (**Figure 4**). The cell density of the retinal ganglion cell layer decreased significantly in the S961 group at 24 days with a mean difference of 1412 cells/mm^2 compared with baseline ($P < 0.001$), and a mean difference of 1020 cells/mm^2 between experimental and control groups at 24 days ($P < 0.001$). An apparent increase in the size of nuclei was also observed in the S961 group, indicating apoptosis. No significant difference was observed in the average retinal ganglion cell density between experimental and control eyes at baseline ($P = 0.712$). These retinal changes were accompanied by peripapillary atrophy identified as loss of reddish flush and ensuing pallor around the optic nerve head by color fundus photography (**Figure 5**).

The effects of S961 on the expression of InR, GFAP, AQP4, TNFα, and OPA1 were also investigated in the eye and optic nerve (**Figures 5–7**). In the retina, there was a significant increase in GFAP expression across the retinal layers at 24 days after S961 injection when compared to baseline ($P < 0.001$), while no significant change was observed in the control group between baseline and 24 days (**Figure 4**). The experimental S961 group also showed a significant decrease in InR expression in the retinal ganglion cell layer at 24 days ($P < 0.001$) but an opposite trend of increased InR expression in the photoreceptor layer ($P < 0.001$; **Figure 4**). In the optic nerve, there was a significant increase in TNFα and OPA1 expression at 24 days after S961 injection compared with baseline ($P < 0.001$), while no significant change was observed in the control group between baseline and 24 days (**Figure 5B** and **C**).

In the ciliary bodies, a significant increase in AQP4 expression was observed in the experimental S961 group ($P < 0.001$), but not the control group ($P > 0.05$) at 24 days after intracerebroventricular injection (**Figure 6**). In contrast, in the optic nerve, a significant decrease in AQP4 expression was observed in the experimental S961 group at 24 days ($P < 0.001$; **Figure 7**). No significant difference in AQP4 expression was observed in the ciliary bodies or optic nerve of the control group between baseline and 24 days (all $P > 0.05$). In the optic nerve, a significant decrease in InR expression was observed at 24 days in the experimental S961 group ($P < 0.001$), but not the control group ($P > 0.05$) after intracerebroventricular injection. Relative to baseline, increased GFAP and TNFα expression in the optic nerve at 24 days ($P < 0.001$) were also observed in the S961 group but not the control group ($P > 0.05$).

Gene expression changes in the retina
Microarray analysis of the experimental S961 group identified 112 genes that were differentially expressed in the retina compared with controls at 24 days after intracerebroventricular injection (**Figure 8A**). Among these genes, 47 were upregulated and 65 were downregulated significantly. We selected 14 genes involved in neurodegeneration, inflammation, and apoptosis from the list of the significantly dysregulated genes in the microarray analysis for real-time PCR. We observed an upregulation of *IL2*, *IL4*, *FGFR1*, *GSK3a*, and *GSK3b* by 1.98, 2.78, 1.53, 1.60, and 1.22 fold changes respectively, together with a downregulation of *IGF2*, *MAPK15*, *NFKB1A*, *PI3K*, *NRG1*, *BCL2L11*, *IGF1*, *RARB*, and *InR* by 2.35, 1.65, 2.39, 2.07, 2.05, 1.94, 1.55, 2.14, and 3.30 fold changes (all $P < 0.05$) respectively (**Figure 8B**).

Networks and pathways involved in the retina
MetaCore analysis of remarkably up/downregulated genes post-S961 injection revealed that the major canonical pathways altered could be mediated through *IL15*, *NF-kB*, *TREM2-ApoE*, and *Akt-PI3K*, which played a role in apoptosis, immune response, microglial activation, and *mTOR* regulation respectively (**Figure 8C**). Moreover, the remarkably up/downregulated genes post-S961 injection were enriched with functions related to selective glutamate receptor activity, cholinergic activity, protein complex assembly in synapse maturation, cell cycle regulation, and stimulus response. Further network analysis revealed that the upregulated genes *NGFR* and *BNP* interacted with *NF-kbA1* through *PPAR-gamma* (**Figure 8C**).

Discussion

Around 16–47 percent of the world adult population has been estimated to have insulin resistance (Fahed et al., 2020). This condition predisposes to diabetes, neuropathy, nephropathy, dementia, and metabolic syndrome, and compromises the quality of life (Saboya et al., 2016). However, its role in the ocular tissues has largely been understudied. While the role of insulin resistance in neurodegenerative diseases is now being recognized, considering the eye and optic nerve as an extension of the brain, it is possible that central insulin resistance may be involved in the degenerative processes of the retina and optic nerve (Dada, 2017; Faiq and Dada, 2017; Agostinone et al., 2018; Al Hussein Al Awamlh et al., 2021). In this study, we report pathological changes in the anterior segment, retina, and optic nerve upon central insulin resistance by S961 in rodents. S961 is a peptide that binds specifically to InR. Here, intracerebroventricular S961 injection downregulated insulin signaling without systemic disturbance to insulin production or glucose utilization. This isolated insulin resistance in the central nervous system by S961 administration provided a novel animal model to understand its effects on the ocular structures and its subsequent neurodegenerative conditions related to vision, independent of overt diabetes or hyperglycemia.
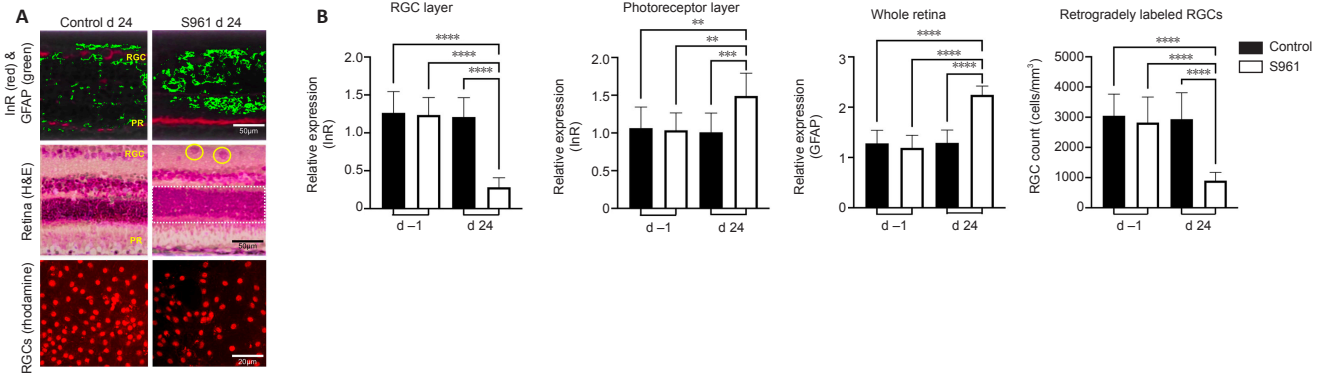
Figure 4 │ Immunohistochemical and cellular alterations in the retina.
(A) (Top row) Immunofluorescence images showing glial fibrillary acidic protein (GFAP) (green) and insulin receptor (InR) (red) expression of retinal cross sections between buffer control (left column) and S961-injected animals (right column) at 24 days after injection. There was a decrease in InR expression in the retinal ganglion cell (RGC) layer and an increase in InR expression in photoreceptor (PR) layer were observed at 24 days in the S961 group. A pan-retinal increase in GFAP expression was also observed in the S961 group compared with the control group. (Middle row) Histological hematoxylin & eosin (H&E) staining of the retinal cross sections revealed a decrease in cell density in the RGC layer in the S961 group compared with the control group at 24 days. Note the dense, enlarged nuclei in the S961 group at 24 days (yellow circles) indicating apoptosis. The outer nuclear layer also showed edema in the S961 group at 24 days (white dotted box) with disorganized cellular architecture in the PR layer. (Bottom row) RGCs retrogradely labeled from the optic nerve using rhodamine labeled dextran amine (red) showed cell count decrease in the S961 group (right) at 24 days compared with the control group. (B) (Leftmost) Relative expression of InR in the RGC layer in the experimental S961 group (white) and buffer control group (black) at −1 day (baseline) and 24 days. There was a significant decrease in InR expression in the RGC layer for the S961 group at 24 days. (Middle left) Relative expression of InR in the PR layer of both groups at −1 and 24 days, with a significant increase in InR expression in PR layer in the S961 group. (Middle right) Relative expression of GFAP in the whole retina in the experimental and control groups at −1 and 24 days, with a significant increase in GFAP expression after S961 injection. (Rightmost) Absolute cell number counts in RGCs using rhodamine labelled dextran amine showed significant RGC loss in the S961 group at 24 days compared with baseline and the control group at 24 days. Results are presented as the mean ± SEM with $n = 6$ per group (two-way analysis of variance followed by Tukey's honest significant difference *post hoc* test: **P < 0.01, ***P < 0.001, ****P < 0.0001; experiments were run in triplicate).
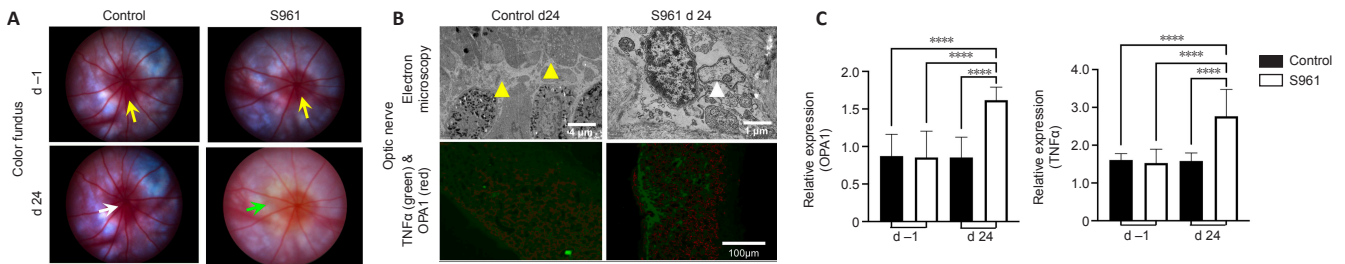

Figure 5 │ Color fundus photography and electron microscopy of the optic nerve.
(A) Color fundus photographs of the control (left column) and S961-injected (right column) animals at −1 day (d −1; baseline; upper row) and 24 days (d 24; lower row). At −1 day, the images showed distinct boundaries of the optic nerve head (yellow arrows) and a reddish flush (white arrow) indicative of intact microvasculature in both groups. At 24 days, the S961 group showed a lack of distinct boundary in the retina (green arrow) at the peripapillary region, suggestive of optic nerve edema in agreement with histology in Figure 4. The reddish flush was also less apparent in the S961 group at 24 days indicative of disruption of microvascular integrity. (B) (Upper row) Transmission electron micrographs showed intact cellular architecture (yellow arrowheads) in the optic nerve head of control group (left) at 24 days while there were degenerative changes with fibroblast infiltration (white arrowhead) in the S961 group at 24 days (right). (Lower row) Immunofluorescence images showed the differential expression of tumor necrosis factor alpha (TNFα) (green) and optic atrophic factor 1 (OPA1) (red) near the optic nerve head, with higher expression in the S961 group (right) than the control group (left) at 24 days. (C) Quantitative analysis of the relative expression of OPA1 (left) and TNFα (right) in the optic nerve head at −1 (baseline) and 24 days in the control (black) and S961 groups (white), showing a significant increase in both OPA1 and TNFα expression in the S961 group at 24 days. Results are presented as the mean ± SEM with $n = 6$ per group (two-way analysis of variance followed by Tukey's honest significant difference *post hoc* test: ****P < 0.0001; experiments were run in triplicate).
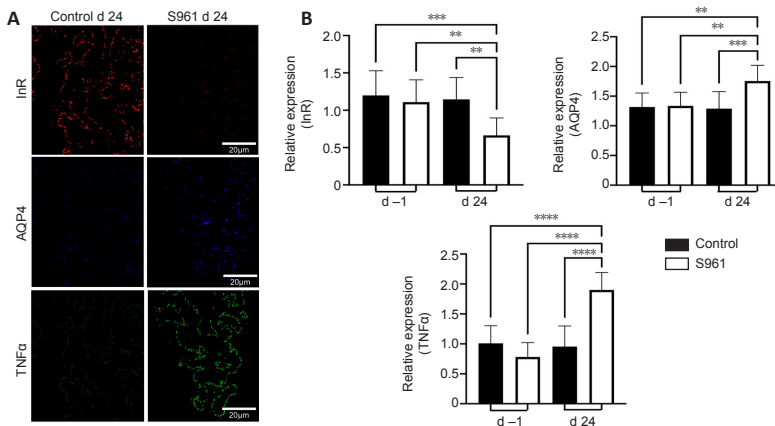

Figure 6 │ Immunohistochemical changes in the ciliary bodies.
(A) Immunofluorescence images of the ciliary bodies showing the expression of insulin receptor (InR) (top row; red), aquaporin-4 (AQP4) (middle row; blue) and tumor necrosis factor alpha (TNFα) (bottom row; green) in the buffer control group (left column) and the experimental S961 group (right column) at 24 days. A marked decrease in InR and increases in AQP4 and TNFα expression were apparent in the S961 group as compared to the buffer control. (B) Quantitative analysis of the relative expression of InR (top), AQP4 (middle), and TNFα (bottom) in the ciliary bodies of the control (black) and S961 groups (white) at −1 day (baseline) and 24 days, showing a significant decrease in InR and increases in AQP4 and TNFα expression in the S961 group at 24 days. Results are presented as the mean ± SEM with $n = 6$ per group. (Two-way analysis of variance followed by Tukey's honest significant difference *post hoc* test: **P < 0.01, ***P < 0.001, ****P < 0.0001; experiments were run in triplicate).
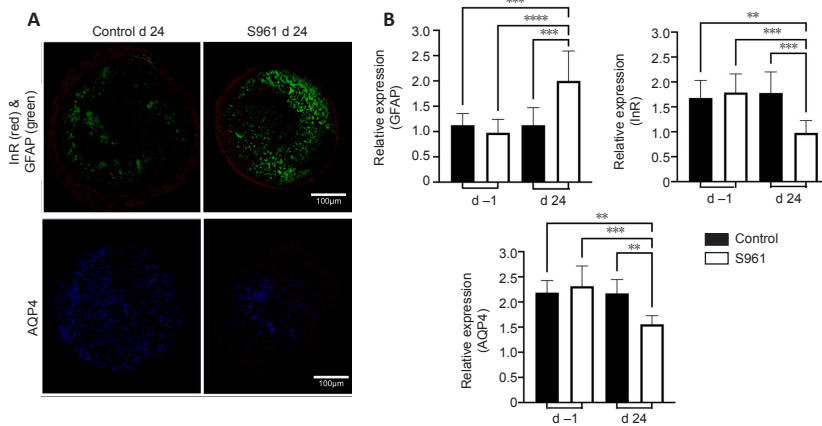
Figure 7 | Immunohistochemical changes in the optic nerve.
(A) Immunofluorescence images of optic nerve cross section showing the expression of InR (top row, red), GFAP (top row, green), and AQP4 (bottom row, blue) in the control group (left column) and the S961 group (right column) at 24 days, with higher GFAP, and lower InR and AQP4 expression being observed in the S961 group relative to the buffer control. (B) Quantitative analysis of the relative expression of GFAP (top left), InR (top right), and AQP4 (bottom) in the optic nerve of the experimental S961 group (white) and buffer control group (black) at −1 day (baseline) and 24 days. There was a significant increase in GFAP expression and significant decreases in InR and AQP4 expression being detected in the optic nerve in the S961 group at 24 days. Results are presented as the mean ± SEM with n = 6 per group (two-way analysis of variance followed by Tukey's honest significant difference *post hoc* test: **P < 0.01, ***P < 0.001, ****P < 0.0001; experiments were run in triplicate). AQP4: Aquaporin 4; GFAP: glial fibrillary acidic protein.
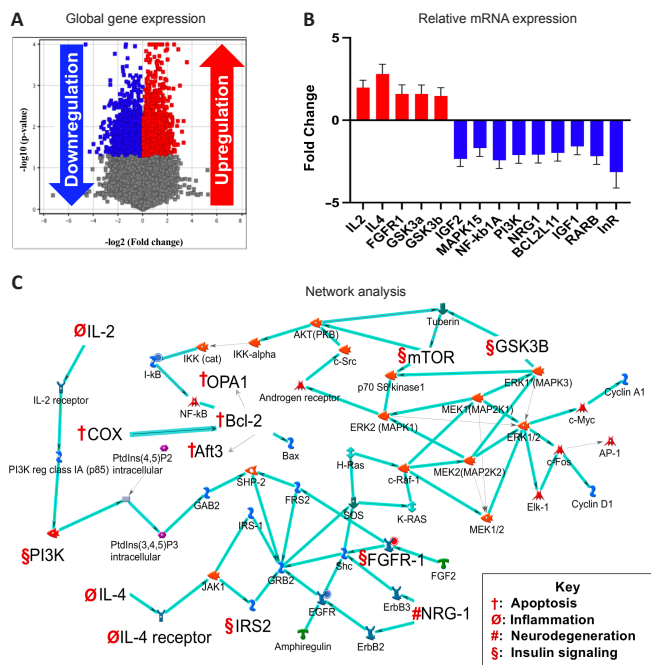
Figure 8 | Gene expression and network analyses.
(A) Volcano plot showing the gene expression pattern in terms of fold change in the retina at 24 days after intracerebroventricular S961 injection. Each dot represents a gene with blue (downregulation) and red (upregulation) indicating genes that had significantly changed expression (unpaired *t*-tests, P < 0.05). Out of the 17,295 genes mapped using the Affymetrix RaGene-1_0-st-v1-type arrays, 65 were upregulated (red) and 47 were downregulated (blue). (B) A selected cohort of 14 dysregulated genes from A was further validated with real-time polymerase chain reaction analysis where interleukin 2 (*IL2*), interleukin 4 (*IL4*), fibroblast growth factor receptor 1 (*FGFR1*), glycogen synthase kinase 3a (*GSK3a*), and glycogen synthase kinase 3b (*GSK3b*) were upregulated (red) and insulin like growth factor 2 (*IGF2*), mitogen-activated protein kinase 15 (*MAPK15*), nuclear factor kappa B1A (*NF-kb1A*), phosphatidylinositol 3-kinase (*PI3K*), neuregulin 1 (*NRG1*), *BCL2L11*, insulin like growth factor 1 (*IGF1*), retinoic acid receptor beta (*RARB*) and insulin receptor (*InR*) were downregulated (blue) (all P < 0.05). Results are expressed as the mean ± SEM. (C) Network analysis showing highly scored network from statistical analysis for MetaCore with thick cyan lines indicating parts of canonical pathways (n = 6). *Aft3*: Activating transcription factor 3; *COX*: cyclooxygenase; *IRS2*: insulin receptor substrate 2; *mTOR*: mechanistic target of rapamycin kinase; *OPA1*: optic atrophy factor 1.

Owing to the expression of InR in various ocular tissues (Naeser, 1997; Reiter and Gardner, 2003), insulin resistance has been implicated in ocular health (Cheung and Wong, 2007) including intraocular pressure elevation (Oh et al., 2005), optic nerve diseases (Roddy, 2020), glaucoma (Gasser et al., 1999), macular degeneration (Zhang et al., 2016), and diabetic retinopathy (Heidari, 2015). Nevertheless, there is no direct evidence for its causality (Faiq et al., 2014). Since dysfunction of the trabecular meshwork and ciliary body and the consequent disruption of the aqueous humor dynamics can result in intraocular pressure elevation and potentially glaucoma, our results of morphological changes in the trabecular meshwork and immunohistochemical changes in both the trabecular meshwork and ciliary body after S961 administration provide mechanistic insights into how insulin resistance may underpin the causality for intraocular pressure elevation and the consequent glaucomatous damages. Whether the intracerebroventricular

injection procedures caused any change in intracranial pressure that led to intraocular pressure elevation is a question that remains to be answered (Ficarrotta and Passaglia, 2020). However, we expect the effects to be small if present, as sham buffer injection did not apparently elevate intraocular pressure at any time points. Our prior dynamic contrast-enhanced magnetic resonance imaging study indicated the entry of the low molecular weight gadolinium contrast agent into the anterior chamber within 30 minutes of intrathecal infusion into healthy adult mice (Faiq et al., 2021a). Given the low molecular weight of S961 at 4804 Da, it is possible that S961 directly reached and influenced the anterior segment of the eye by transporting from the cerebrospinal fluid space to the anterior chamber through the systemic route, whereby the components of peripheral blood enter as a ciliary filtrate into the posterior chamber forming the aqueous humor (Kiel et al., 2011; Ho et al., 2014). S961 might also be transported to the anterior segment through the less recognized subarachnoid trabeculae (Killer et al., 2003; Ohno-Matsui et al., 2011), which presumably connect the optic nerve subarachnoid space to the choroid or suprachoroidal space. The local subarachnoid trabeculae-mediated transport of S961 into the anterior chamber may explain the absence of hyperglycemia or serum insulin change in our experiments, whereas the peripheral blood mediated entry of S961 might play a less dominant role in the ocular changes given its dilution upon systemic circulation. The increase in AQP4 water channel expression in the ciliary bodies and the reduced porosity and AQP4 expression in the trabecular meshwork of the experimental S961 group likely implied increased aqueous inflow and decreased aqueous outflow, respectively (Zhang et al., 2002; Verkman, 2003), that could explain the increase in intraocular pressure after S961 administration.

AQP4 expression can also be found in the rodent optic nerves (Mathieu et al., 2017, 2018; Kimball et al., 2021), while chronic intraocular pressure elevation may not only accompany with altered AQP4 expression (Dibas et al., 2008), but also reduced cerebrospinal fluid entry into the optic nerve (Mathieu et al., 2018; Faiq et al., 2021b). In addition, knocking out AQP4 may reduce amyloid clearance from the optic nerve (Wang et al., 2020). Insulin resistance has been associated with amyloidopathy (Rad et al., 2018), tauopathy (Mullins et al., 2017), glutamate excitotoxicity (Datusalia et al., 2018), inflammation, and neuronal apoptosis in Alzheimer's disease, glaucoma, and maculopathy (Wostyn et al., 2010; Faiq et al., 2014; Ermilov and Nesterova, 2016; Regland and McCaddon, 2019). However, the underlying mechanisms remain unclear. Our current results of the AQP4 decrease, elevation of the inflammatory marker TNFα, and glial activation from GFAP upregulation in the optic nerve after S961 administration suggested a detrimental role of central insulin resistance in the glymphatic brain waste clearance system, which removes toxic metabolites including amyloid via cerebrospinal fluid-interstitial fluid exchange and AQP4 channels in the glia (Iliff et al., 2012; Kasi et al., 2022). Changes in gene expression involved in insulin signaling, inflammatory markers, and neurodegenerative phenotypes indicate that central insulin resistance may be a cardinal feature of degenerative diseases of vision. Together with the retinal vascular dysregulation, retinal ganglion cell loss, and mitochondrial damage from OPA1 elevation in the optic nerve of the experimental S961 group, our results suggest the need to examine if central insulin resistance may be commonly involved in the upstream mechanisms across different retinopathies, optic neuropathies and other conditions involving vision.

With evidence from physiological, biochemical, molecular, genetic, and histological dimensions, this study supports the role of central insulin resistance in the pathological processes that afflict the visual system. There are, however, important questions that remain to be addressed, such as the gender effects on the severity of insulin resistance given the different body compositions and adipose tissue distributions (Geer and Shen, 2009). It is worth noting that difference between sexes exists in Alzheimer's disease (Mielke, 2018) while there is a reported spike in the incidence of glaucoma in postmenopausal women (Dewundara et al., 2016). On the other hand,

rodents do not have lamina cribrosa and their AQP4 expression in the optic nerve is different from that of humans (Kimball et al., 2021). Thus, cautions are warranted in the context of direct clinical translations of the current results. Apart from intracerebroventricular injection, direct injection of S961 into the eye via intracameral, intravitreal, subretinal or suprachoroidal route could provide additional insights towards understanding the mechanisms of insulin resistance in ocular health and disease. Longitudinal ocular and brain imaging (e.g. optical coherence tomography and magnetic resonance imaging) and behavioral assessments (e.g. optokinetic and optomotor response measurements) could add mechanistic insights into the central insulin resistance-related changes within and beyond the visual system over time (Yang et al., 2018; van der Merwe et al., 2021; Zhu et al., 2021). Future studies may also consider alternative animal models such as the neuronal InR knockout (NIRKO) mice (Schubert et al., 2004) to determine more specific mechanisms of ocular and vision-related alterations in the absence of InR.

To conclude, our study indicates that insulin resistance in the central nervous system can exist independent of systemic insulin resistance or overt diabetes. We also provide evidence that central insulin resistance may play a role in aqueous humor dynamics, intraocular pressure elevation, inflammation, vascular dysregulation, mitochondrial dysfunction, and retinal and optic nerve damages. Since insulin resistance is on rise and a significant percentage of the world population is suffering from this condition, it becomes important to determine its impact on neurodegenerative conditions through genetic and biochemical pathways. Taken together, our results suggested central insulin resistance a possible underlying condition for diseases of vision and urge the need to explore novel insulin-based treatment options, given the initial evidence that insulin plays an anti-inflammatory role in the central nervous system (Ferreira et al., 2014; Rodriguez-Casado et al., 2017) with intrinsic capacity to regenerate dendrites and synapses after injury (Agostinone et al., 2018). The role of neuroprotective agents, insulin sensitizing agents, and ocular hypotensives in isolation or combination could be considered for additional therapeutic advantage to relevant disorders of the visual system (Downs et al., 2022; Sanchez-Cruz et al., 2022; Wareham et al., 2022). Future studies may also determine if other novel therapeutics such as mindfulness meditation may alleviate insulin resistance along with other major risk factors in neurodegenerative diseases of the visual system including glaucoma (Dada et al., 2018; Sabel et al., 2018).

References

Agostinone J, Alarcon-Martinez L, Gamlin C, Yu WQ, Wong ROL, Di Polo A (2018) Insulin signalling promotes dendrite and synapse regeneration and restores circuit function after axonal injury. Brain 141:1963-1980.

Al Hussein Al Awamlh S, Wareham LK, Risner ML, Calkins DJ (2021) Insulin signaling as a therapeutic target in glaucomatous neurodegeneration. Int J Mol Sci 22:4672.

Arnold SE, Arvanitakis Z, Macauley-Rambach SL, Koenig AM, Wang HY, Ahima RS, Craft S, Gandy S, Buettner C, Stoeckel LE, Holtzman DM, Nathan DM (2018) Brain insulin resistance in type 2 diabetes and Alzheimer disease: concepts and conundrums. Nat Rev Neurol 14:168-181.

Bao YK, Yan Y, Wilson B, Gordon MO, Semenkovich CF, Rajagopal R (2020) Association of retinopathy and insulin resistance: NHANES 2005-2008. Curr Eye Res 45:173-176.

Barishak YR (1992) Embryology of the eye and its adnexae. Dev Ophthalmol 24:1-142.

Boothroyd CE, Wijnen H, Naef F, Saez L, Young MW (2007) Integration of light and temperature in the regulation of circadian gene expression in Drosophila. PLoS Genet 3:e54.

Bronson SK, Reiter CE, Gardner TW (2003) An eye on insulin. J Clin Invest 111:1817-1819.

Cheung N, Wong TY (2007) Obesity and eye diseases. Surv Ophthalmol 52:180-195.

Cvekl A, Tamm ER (2004) Anterior eye development and ocular mesenchyme: new insights from mouse models and human diseases. Bioessays 26:374-386.

Dada T (2017) Is glaucoma a neurodegeneration caused by central insulin resistance: diabetes type 4? J Curr Glaucoma Pract 11:77-79.

Dada T, Mittal D, Mohanty K, Faiq MA, Bhat MA, Yadav RK, Sihota R, Sidhu T, Velpandian T, Kalaivani M, Pandey RM, Gao Y, Sabel BA, Dada R (2018) Mindfulness meditation reduces intraocular pressure, lowers stress biomarkers and modulates gene expression in glaucoma: a randomized controlled trial. J Glaucoma 27:1061-1067.

Datusalia AK, Agarwal P, Singh JN, Sharma SS (2018) Hyper-insulinemia increases the glutamate-excitotoxicity in cortical neurons: A mechanistic study. Eur J Pharmacol 833:524-530.

Dewundara SS, Wiggs JL, Sullivan DA, Pasquale LR (2016) Is estrogen a therapeutic target for glaucoma? Semin Ophthalmol 31:140-146.

Dibas A, Yang MH, He S, Bobich J, Yorio T (2008) Changes in ocular aquaporin-4 (AQP4) expression following retinal injury. Mol Vis 14:1770-1783.

Downs JC, Fleischman D; 2020–2022 Research Committee of the American Glaucoma Society and the 2020–2022 Glaucoma Clinical Committee of the American Society of Cataract and Refractive Surgery (2022) Unmet Needs in the Detection, Diagnosis, Monitoring, Treatment, and Understanding of Primary Open-Angle Glaucoma: A Position Statement of the American Glaucoma Society and the American Society of Cataract and Refractive Surgery. Ophthalmol Glaucoma S2589-4196(22)00026-6.

Ermilov VV, Nesterova AA (2016) Beta-amyloidopathy in the pathogenesis of age-related macular degeneration in correlation with neurodegenerative diseases. Adv Exp Med Biol 854:119-125.

Fahed M, Abou Jaoudeh MG, Merhi S, Mosleh JMB, Ghadieh R, Al Hayek S, El Hayek Fares JE (2020) Evaluation of risk factors for insulin resistance: a cross sectional study among employees at a private university in Lebanon. BMC Endocr Disord 20:85.

Faiq MA, Dada R, Saluja D, Dada T (2014) Glaucoma--diabetes of the brain: a radical hypothesis about its nature and pathogenesis. Med Hypotheses 82:535-546.

Faiq MA, Dada R, Kumar A, Saluja D, Dada T (2016) Brain: the potential diagnostic and therapeutic target for glaucoma. CNS Neurol Disord Drug Targets 15:839-844.

Faiq MA, Dada T (2017) Diabetes type 4: a paradigm shift in the understanding of glaucoma, the brain specific diabetes and the candidature of insulin as a therapeutic agent. Curr Mol Med 17:46-59.

Faiq MA, Adi V, Khoja S, Sainulabdeen A, Chan RW, Parra C, Hamilton-Fletcher G, Lee CH, Zhang J, Wollstein G, Schuman JS, Chan KC (2021a) Entry of cerebrospinal fluid components into the anterior chamber of the eye. Invest Ophthalmol Vis Sci 62:37.

Faiq MA, Adi V, Zhu J, Khoja S, Sainulabdeen A, Parra C, Hamilton-Fletcher G, Lee CH, Zhang J, Leung CK, Wollstein G, Schuman JS, Chan KC (2021b) Effects of chronic intraocular pressure elevation on cerebrospinal fluid dynamics in the optic nerve. Invest Ophthalmol Vis Sci 62:1861.

Ferreira ST, Clarke JR, Bomfim TR, De Felice FG (2014) Inflammation, defective insulin signaling, and neuronal dysfunction in Alzheimer's disease. Alzheimers Dement 10:S76-83.

Ferry B, Gervasoni D (2021) Improving stereotaxic neurosurgery techniques and procedures greatly reduces the number of rats used per experimental group-a practice report. Animals (Basel) 11:2662.

Ficarrotta KR, Passaglia CL (2020) Intracranial pressure modulates aqueous humour dynamics of the eye. J Physiol 598:403-413.

Galvis V, Lopez-Jaramillo P, Tello A, Castellanos-Castellanos YA, Camacho PA, Cohen DD, Gomez-Arbelaez D, Merayo-Lloves J (2016) Is myopia another clinical manifestation of insulin resistance? Med Hypotheses 90:32-40.

Gasser P, Stumpfig D, Schotzau A, Ackermann-Liebrich U, Flammer J (1999) Body mass index in glaucoma. J Glaucoma 8:8-11.

Geer EB, Shen W (2009) Gender differences in insulin resistance, body composition, and energy balance. Gend Med 6 Suppl 1:60-75.

Grieb P (2016) Intracerebroventricular streptozotocin injections as a model of Alzheimer's disease: in search of a relevant mechanism. Mol Neurobiol 53:1741-1752.

Heidari B (2015) Obesity and diabetic retinopathy: What is the association? Caspian J Intern Med 6:184-186.

Ho LC, Conner IP, Do CW, Kim SG, Wu EX, Wollstein G, Schuman JS, Chan KC (2014) In vivo assessment of aqueous humor dynamics upon chronic ocular hypertension and hypotensive drug treatment using gadolinium-enhanced MRI. Invest Ophthalmol Vis Sci 55:3747-3757.

Iliff JJ, Wang M, Liao Y, Plogg BA, Peng W, Gundersen GA, Benveniste H, Vates GE, Deane R, Goldman SA, Nagelhus EA, Nedergaard M (2012) A paravascular pathway facilitates CSF flow through the brain parenchyma and the clearance of interstitial solutes, including amyloid beta. Sci Transl Med 4:147ra111.

Kasi A, Liu C, Faiq MA, Chan KC (2022) Glymphatic imaging and modulation of the optic nerve. Neural Regen Res 17:937-947.

Kermani SK, Khatony A, Jalali R, Rezaei M, Abdi A (2017) Accuracy and precision of measured blood sugar values by three glucometers compared to the standard technique. J Clin Diagn Res 11:OC05-OC08.

Kiel JW, Hollingsworth M, Rao R, Chen M, Reitsamer HA (2011) Ciliary blood flow and aqueous humor production. Prog Retin Eye Res 30:1-17.

Killer HE, Laeng HR, Flammer J, Groscurth P (2003) Architecture of arachnoid trabeculae, pillars, and septa in the subarachnoid space of the human optic nerve: anatomy and clinical considerations. Br J Ophthalmol 87:777-781.

Kimball E, Schaub J, Quillen S, Keuthan C, Pease ME, Korneva A, Quigley H (2021) The role of aquaporin-4 in optic nerve head astrocytes in experimental glaucoma. PLoS One 16:e0244123.

Lamb TD, Collin SP, Pugh EN, Jr. (2007) Evolution of the vertebrate eye: opsins, photoreceptors, retina and eye cup. Nat Rev Neurosci 8:960-976.

Langenberg T, Kahana A, Wszalek JA, Halloran MC (2008) The eye organizes neural crest cell migration. Dev Dyn 237:1645-1652.

Lee YS, Chen CH, Tsai CN, Tsai CL, Chao A, Wang TH (2009) Microarray labeling extension values: laboratory signatures for Affymetrix GeneChips. Nucleic Acids Res 37:e61.

Liu L, Jiang Y, Curtiss E, Fukuchi KI, Steinle JJ (2017) TLR4 regulates insulin-resistant proteins to increase apoptosis in the mouse retina. Inflamm Res 66:993-997.

Livak KJ, Schmittgen TD (2001) Analysis of relative gene expression data using real-time quantitative PCR and the 2(-Delta Delta C(T)) Method. Methods 25:402-408.

Mathieu E, Gupta N, Ahari A, Zhou X, Hanna J, Yucel YH (2017) Evidence for cerebrospinal fluid entry into the optic nerve via a glymphatic pathway. Invest Ophthalmol Vis Sci 58:4784-4791.

Mathieu E, Gupta N, Paczka-Giorgi LA, Zhou X, Ahari A, Lani R, Hanna J, Yucel YH (2018) Reduced cerebrospinal fluid inflow to the optic nerve in glaucoma. Invest Ophthalmol Vis Sci 59:5876-5884.

Mielke MM (2018) Sex and gender differences in Alzheimer's disease dementia. Psychiatr Times 35:14-17.

Moreira-Silva D, Vizin RCL, Martins TMS, Ferreira TL, Almeida MC, Carrettiero DC (2019) Intracerebral injection of streptozotocin to model Alzheimer disease in rats. Bio Protoc 9:e3397.

Mullins RJ, Diehl TC, Chia CW, Kapogiannis D (2017) Insulin resistance as a link between amyloid-beta and tau pathologies in Alzheimer's disease. Front Aging Neurosci 9:118.

Nadal-Nicolás FM, Salinas-Navarro M, Vidal-Sanz M, Agudo-Barriuso M (2015) Two methods to trace retinal ganglion cells with fluorogold: from the intact optic nerve or by stereotactic injection into the optic tract. Exp Eye Res 131:12-19.

Naeser P (1997) Insulin receptors in human ocular tissues. Immunohistochemical demonstration in normal and diabetic eyes. Ups J Med Sci 102:35-40.

Oh SW, Lee S, Park C, Kim DJ (2005) Elevated intraocular pressure is associated with insulin resistance and metabolic syndrome. Diabetes Metab Res Rev 21:434-440.

Ohno-Matsui K, Akiba M, Moriyama M, Ishibashi T, Tokoro T, Spaide RF (2011) Imaging retrobulbar subarachnoid space around optic nerve by swept-source optical coherence tomography in eyes with pathologic myopia. Invest Ophthalmol Vis Sci 52:9644-9650.

Okoniewski MJ, Hey Y, Pepper SD, Miller CJ (2007) High correspondence between Affymetrix exon and standard expression arrays. Biotechniques 42:181-185.

Patel SS, Mehta V, Changotra H, Udayabanu M (2016) Depression mediates impaired glucose tolerance and cognitive dysfunction: a neuromodulatory role of rosiglitazone. Horm Behav 78:200-210.

Pohl AA, Sugnet CW, Clark TA, Smith K, Fujita PA, Cline MS (2009) Affy exon tissues: exon levels in normal tissues in human, mouse and rat. Bioinformatics 25:2442-2443.

Rad SK, Arya A, Karimian H, Madhavan P, Rizwan F, Koshy S, Prabhu G (2018) Mechanism involved in insulin resistance via accumulation of beta-amyloid and neurofibrillary tangles: link between type 2 diabetes and Alzheimer's disease. Drug Des Devel Ther 12:3999-4021.

Rajagopal R, Bligard GW, Zhang S, Yin L, Lukasiewicz P, Semenkovich CF (2016) Functional deficits precede structural lesions in mice with high-fat diet-induced diabetic retinopathy. Diabetes 65:1072-1084.

Regland B, McCaddon A (2019) Alzheimer's amyloidopathy: an alternative aspect. J Alzheimers Dis 68:483-488.

Reiter CE, Gardner TW (2003) Functions of insulin and insulin receptor signaling in retina: possible implications for diabetic retinopathy. Prog Retin Eye Res 22:545-562.

Roddy GW (2020) Metabolic syndrome is associated with ocular hypertension and glaucoma. J Glaucoma 29:726-731.

Rodriguez-Casado A, Toledano-Diaz A, Toledano A (2017) Defective insulin signalling, mediated by inflammation, connects obesity to alzheimer disease; relevant pharmacological therapies and preventive dietary interventions. Curr Alzheimer Res 14:894-911.

Sabel BA, Wang J, Cardenas-Morales L, Faiq M, Heim C (2018) Mental stress as consequence and cause of vision loss: the dawn of psychosomatic ophthalmology for preventive and personalized medicine. EPMA J 9:133-160.

Saboya PP, Bodanese LC, Zimmermann PR, Gustavo AD, Assumpcao CM, Londero F (2016) Metabolic syndrome and quality of life: a systematic review. Rev Lat Am Enfermagem 24:e2848.

Sanchez-Cruz A, Hernandez-Pinto A, Lillo C, Isiegas C, Marchena M, Lizasoain I, Bosch F, de la Villa P, Hernandez-Sanchez C, de la Rosa EJ (2022) Insulin receptor activation by proinsulin preserves synapses and vision in retinitis pigmentosa. Cell Death Dis 13:383.

Schneider CA, Rasband WS, Eliceiri KW (2012) NIH Image to ImageJ: 25 years of image analysis. Nat Methods 9:671-675.

Schubert M, Gautam D, Surjo D, Ueki K, Baudler S, Schubert D, Kondo T, Alber J, Galldiks N, Kustermann E, Arndt S, Jacobs AH, Krone W, Kahn CR, Bruning JC (2004) Role for neuronal insulin resistance in neurodegenerative diseases. Proc Natl Acad Sci U S A 101:3100-3105.

Seyer B, Pham V, Albiston AL, Chai SY (2016) Cannula implantation into the lateral ventricle does not adversely affect recognition or spatial working memory. Neurosci Lett 628:171-178.

Talbot K (2014) Brain insulin resistance in Alzheimer's disease and its potential treatment with GLP-1 analogs. Neurodegener Dis Manag 4:31-40.

van der Merwe Y, Murphy MC, Sims JR, Faiq MA, Yang XL, Ho LC, Conner IP, Yu Y, Leung CK, Wollstein G, Schuman JS, Chan KC (2021) Citicoline modulates glaucomatous neurodegeneration through intraocular pressure-independent control. Neurotherapeutics 18:1339-1359.

Verkman AS (2003) Role of aquaporin water channels in eye function. Experimental eye research 76:137-143.

Wang X, Lou N, Eberhardt A, Yang Y, Kusk P, Xu Q, Förstera B, Peng S, Shi M, Ladrón-de-Guevara A, Delle C, Sigurdsson B, Xavier ALR, Ertürk A, Libby RT, Chen L, Thrane AS, Nedergaard M (2020) An ocular glymphatic clearance system removes β-amyloid from the rodent eye. Sci Transl Med 12:eaaw3210.

Wareham LK, Liddelow SA, Temple S, Benowitz LI, Di Polo A, Wellington C, Goldberg JL, He Z, Duan X, Bu G, Davis AA, Shekhar K, Torre A, Chan DC, Canto-Soler MV, Flanagan JG, Subramanian P, Rossi S, Brunner T, Bovenkamp DE, et al. (2022) Solving neurodegeneration: common mechanisms and strategies for new treatments. Mol Neurodegener 17:23.

Wohlfart P, Lin J, Dietrich N, Kannt A, Elvert R, Herling AW, Hammes HP (2014) Expression patterning reveals retinal inflammation as a minor factor in experimental retinopathy of ZDF rats. Acta Diabetol 51:553-558.

Wostyn P, Audenaert K, De Deyn PP (2010) Alzheimer's disease: cerebral glaucoma? Med Hypotheses 74:973-977.

Yang XL, van der Merwe Y, Sims J, Parra C, Ho LC, Schuman JS, Wollstein G, Lathrop KL, Chan KC (2018) Age-related changes in eye, brain and visuomotor behavior in the DBA/2J mouse model of chronic glaucoma. Sci Rep 8:4643.

Zarei R, Anvari P, Eslami Y, Fakhraie G, Mohammadi M, Jamali A, Afarideh M, Ghajar A, Heydarzade S, Esteghamati A, Moghimi S (2017) Retinal nerve fibre layer thickness is reduced in metabolic syndrome. Diabet Med 34:1061-1066.

Zhang D, Vetrivel L, Verkman AS (2002) Aquaporin deletion in mice reduces intraocular pressure and aqueous fluid production. J Gen Physiol 119:561-569.

Zhang QY, Tie LJ, Wu SS, Lv PL, Huang HW, Wang WQ, Wang H, Ma L (2016) Overweight, obesity, and risk of age-related macular degeneration. Invest Ophthalmol Vis Sci 57:1276-1283.

Zhu J, Sainulabdeen A, Akers K, Adi V, Sims JR, Yarsky E, Yan Y, Yu Y, Ishikawa H, Leung CK, Wollstein G, Schuman JS, Wei W, Chan KC (2021) Oral scutellarin treatment ameliorates retinal thinning and visual deficits in experimental glaucoma. Front Med (Lausanne) 8:681169.